Research on the Physical Properties and Microstructure Of Refractory Blocks Used in Combustion Cell

Jian Chen [1*] ,Qiang Xue [2] ,Hua Li [1] ,Senqi Pei [1] ,Xincheng Wang [3] ,Ping Yuan [4]

[1]Southwest Oil & Gas Field Company Northwest Sichuan Gas Mine, Mian Yang, China
[2] Infrastructure Engineering Department of Southwest Oil & Gas Field Company, Mian Yang , China
[3] Tight Oil and Gas Exploration and Development Project Department of Southwest Oil and Gas Field Company, Mian Yang , China
[4]Sichuan Kehong Petroleum and Natural Gas Engineering Co. , Ltd, Cheng Du , China

* Corresponding author.E-mail address: cj198427@petrochina.com.cn.

Abstract. Exposure to high temperatures is one of the most important deterioration processes of building structures during their service life. In order to understand the changes in the working capacity of refractory blocks used in oil drilling and arson operations, samples were taken of refractory blocks that had been heat treated and not heat treated in the spray cell, the physical and chemical properties, phase composition, microstructure, etc. of the samples were analyzed and studied. The results show that when refractory blocks are sintered under high temperature, the aluminate, aluminum phosphate, etc. of the internal cementing materials will decompose, forming Al_2O_3 as a loose and porous structure. After high temperature treatment in the combustion cell, the internal structure and composition of the refractory blocks have better Thermal stability, volume and thermal conductivity basically do not change under the condition of 1200℃; the compressive strength and flexural strength of unheated refractory blocks are 20. 56Mpa and 3. 1Mpa respectively. Heat treatment makes the compressive strength and flexural strength of refractory blocks respectively. Reduced by 21. 52% and 43. 01%. The research results provide a reference for the service performance of refractory blocks during the use of combustion cell.

Keywords: refractory blocks, compressive strength, flexural strength, microstructure

1 INTRODUCTION

The natural gas combustion cell is a masonry structure, reinforced concrete structure or mixed structure enclosed on three sides, which is built to avoid the impact of natural gas combustion on the surrounding environment during blowout [1]. Domestic combustion cells are mostly made of shale blocks, supplemented by M10 cement mortar bonding[2]. During the blasting process of shale clay blocks, the wing wall often cracks or

B. Yuan et al. (eds.), *Proceedings of the 2024 8th International Conference on Civil Architecture and Structural Engineering (ICCASE 2024)*, Atlantis Highlights in Engineering 33,
https://doi.org/10.2991/978-94-6463-449-5_31

part of the cell wall melts, which poses safety risks and cannot meet the requirements of long-term blasting [3]. With the large-scale oil and gas exploration work in western China, refractory blocks made of amorphous refractory materials have become the main building materials for the construction of combustion cell. Unshaped refractory materials can be divided into high alumina, magnesia, alumina-magnesia, etc. according to their materials. They are usually composed of aggregates, fine powder, binders and additives[4, 5]. High-aluminum unshaped refractory materials have become the most widely used materials due to their excellent high-temperature performance and economy[6]. The strength of refractory materials is a key parameter that affects their service performance[7]. The failure mechanism of refractory materials under load conditions has always been a hot spot in its research. The unconfined compressive strength test and the flexural strength test are used to quantify the strength value of refractory materials[8, 9].

Based on the above research, a new aluminum phosphate bonded corundum type refractory block was developed. In order to verify the working performance of the new refractory block in the combustion cell, the deterioration mechanism of the block under high temperature was investigated. In this paper, compressive tests, flexural tests and permanent prechange rate tests were carried out on the refractory blocks before and after heat treatment of the combustion tank. The mechanical indexes such as compressive strength, flexural strength and permanent line change rate were investigated. The composition and microstructure of the samples were characterized by X-ray diffraction (XRD) and scanning electron microscopy (SEM).

2 EXPERIMENTAL

The refractory blocks used in the project are made of high-alumina aggregate, corundum powder (≤74μm), aluminate cement, aluminum phosphate, perlite, and aluminum oxide powder. The material mixing ratio is shown in Table 1. The preparation method of the samples involves mixing the raw materials with a controlled amount of water. Subsequently, according to GB/T4513, the mixture is cast into specimens of dimensions 50×50×50mm for compressive strength tests（Figure. 1）, 230×114×64mm for flexural strength tests, and 160×40×40mm for high-temperature permanent linear change tests. The specimens undergo standard curing for a period of 28 days. After curing, half of the samples undergo normal temperature curing, while the other half is placed in a combustion chamber for natural gas ignition in Jianyang, Sichuan, China. The Refractory Block Composition Data is shown in Table 2. The temperature probe measures the average temperature of the samples in the combustion chamber to be 1870°C, with a duration of 267 hours. After the combustion, both heat-treated and untreated samples are subjected to physical performance testing simultaneously.

Table 1. Chemical Composition of Refractory Block Raw Materials

Chemistry Compositions	*Aluminous Cement*	*Calcined Bauxite Aggregate*	*Emery*	*Alumina Powder*	*Aluminium Phosphate*
Al_2O_3 (wt%)	78. 1	81. 65	99. 4	99. 85	29. 8
SiO_2 (wt%)	0. 30	15. 36	0. 06	0. 03	0
CaO (wt%)	19. 5	0. 56	0. 05	0. 02	0
Fe_2O_3 (wt%)	0. 54	2. 83	0. 06	0. 03	0
P_2O_5 (wt%)	0	0	0	0	62. 3

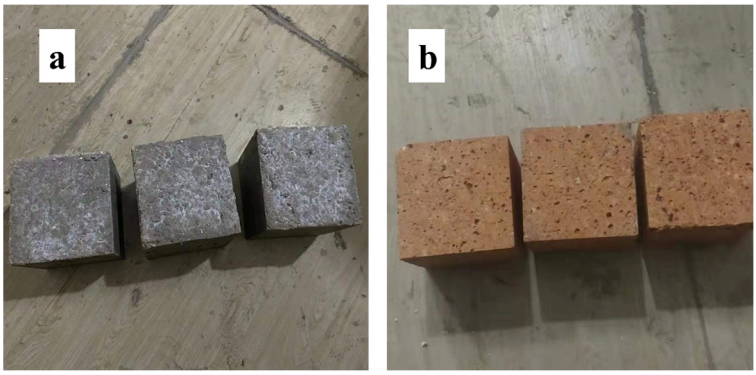

Fig. 1. Unconfined Compressive Strength Specimens. (a) Untreated specimens (b) Specimens after heat treatment.

Table 2. Refractory Block Composition Data

Castabletype	**Unit**	**Quantity**
Aluminous cement CA80	wt%	25
Calcined Bauxite Aggregate	wt%	20
Emery	wt%	20
Aluminium Phosphate	wt%	6
Perlite	wt%	6
Alumina Powder	wt%	4
Maximum Aggregate Size	mm	3
Water Requirement	wt%	19
Open Porosity	vol. %	5. 5
Apparent Density	kg/m^3	2000

2.1 Compressive Strength Test.

In accordance with GB/T5072-2008 "Test method for cold crushing strength of refractory materials, " a 200-ton YAW-2000D computer-controlled electro-hydraulic servo press was used for loading. The test was conducted using displacement-controlled loading at a loading rate of 0. 1mm/min. The test employed a continuous and uniform loading method, with displacement control as the control mode and a set loading rate of

2mm/min. The test was considered concluded when the load dropped to 80% of the peak load, indicating block failure. The formula for calculating axial compressive strength was determined as follows:

$$\sigma = \frac{F}{A} \tag{1}$$

Where σ is Axial Compressive Strength (MPa), F is Peak Load during the specimen loading process (N), A is Loading Surface Area of the specimen (mm²).

2.2 Bending Test

In accordance with GB/T3001-2017 " Refractory products. Determination of modulus of rupture at ambient temperature" a 200-ton YAW-2000D computer-controlled electro-hydraulic servo press was used for loading. The test was conducted using displacement-controlled loading at a constant rate of 0. 6mm/min until the refractory block failed. The flexural strength of the specimen was calculated using the formula and reported with precision to 0. 01MPa.

$$R_c = \frac{3PL}{2BH^2} \tag{2}$$

Where R_c is bending strength (MPa), P is Ultimate Load (N), L is Span Length (mm), B is Sample width (mm), H is Sample height (mm).

2.3 Heating Permanent Line Change Test

In accordance with GB/T 598-2022, “Refractory products—Determination of permanent change in dimensions on heating”, tests were conducted on refractory block specimens at temperatures of 110°C, 400°C, 800°C, and 1200°C, with a heating rate of 5°C/min. The measurement of permanent linear change (Le) during heating is calculated based on the rate of length change before and after heating, as indicated in Formula 3.

$$L_e = \frac{L_1 - L_0}{L_0} \times 100 \tag{3}$$

Where L_e is permanent Linear Change Rate during Heating(%), L_1 is length values at various measuring points after sample heating (mm), L_0 is Length values at various measuring points before sample heating (mm).

2.4 X-ray Diffraction (XRD) Analysis

The experiment was conducted using an X-ray diffractometer manufactured by ZEISS, with a step size of 2θ=0.02 (°)/step and a scanning speed of 5 (°)/minute. Phase quantification was performed using Materials Data's Jade 6.5 software.

2.5 Scanning Electron Microscopy (SEM) Experiment

The experiment was conducted using an Apreo 2C electron microscope manufactured by Thermo Fisher Scientific, operated at 10 kV for image capture. Before the experiment, the central part of the fractured specimen from the unconfined compressive strength test was taken, polished into a sample of dimensions 1cm×0. 5cm×0. 5cm, and subjected to gold sputtering.

3 RESULTS AND DISCUSSION

3.1 Phase Composition and Microstructure

In the refractory material, CA80 aluminate cement is used as aggregate, phosphate is used as coagulant, perlite and alumina powder are used as matrix materials. In the preparation and use of refractory blocks sprayed into the combustion chamber, there are processes such as the hydration of aluminate cement and the sintering of aluminum phosphate. The internal composition and structure of refractory blocks vary significantly at different temperatures. The hydration products of untreated aluminate cement include CA_2、C_3A、C_3AH_6[10, 11], and simultaneously, aluminum oxide and aluminum phosphate phases coexist (Fig.2).

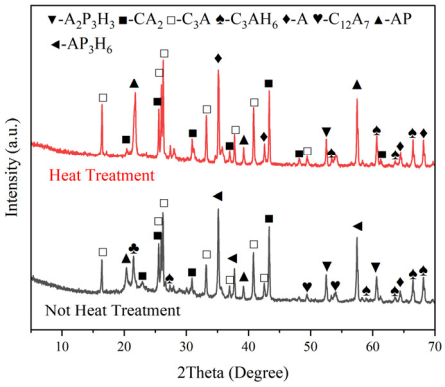

Fig. 2. XRD Spectrum of Refractory Block

Under scanning electron microscopy, diverse forms of hydrated and cementitious substances are observed: granular $Al(H_2PO_4)_3$ enveloping plate-like $AlPO_4$ and cluster-shaped C_3A (Figure.3 a, b, c). This structure provides refractory materials with higher flexural strength. After heat treatment, numerous pores appear in the interior of the refractory material (Figure.3 d, e, f), and substances such as $Al(H_2PO_4)_3$, $AlPO_4$, C_3A lose water and decompose at high temperatures[12, 13]. The structure becomes porous, exhibiting irregular clustered formations.

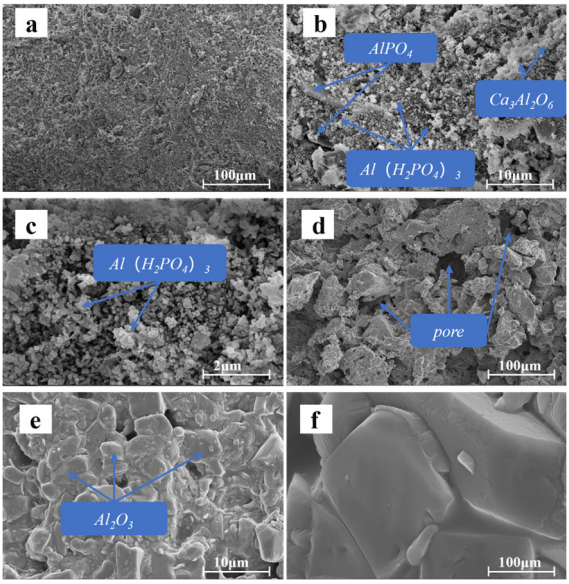

Fig. 3. SEM Images of Refractory Block (a, b, c) Untreated, (d, e, f) Heat Treated

3.2 Physical Properties of the Samples

The high-temperature linear change rate of refractory blocks is shown in Figure 4. The linear change rate of untreated refractory blocks increases with the temperature. Regarding the hydration products of aluminate cement, at 110°C, free water evaporates from the specimen, at 800°C, substances like $Ca(OH)_2$ and $CaCO_3$ decompose into CaO, and at 1200°C, the cement and aggregate melt. Simultaneously, with the increasing heat treatment temperature, aluminum dihydrogen phosphate undergoes phase transformation, converting into $AlPO_4$ and Al_2O_3, resulting in a significant increase in the linear change rate. Generally, the density of the material is positively correlated with macro strength. After heat treatment, refractory blocks have a more porous structure and lower strength.

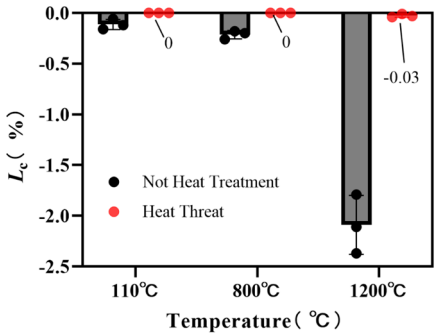

Fig. 4. High-Temperature Permanent Linear Change Rate of Refractory Blocks After Use in the Combustion Chamber

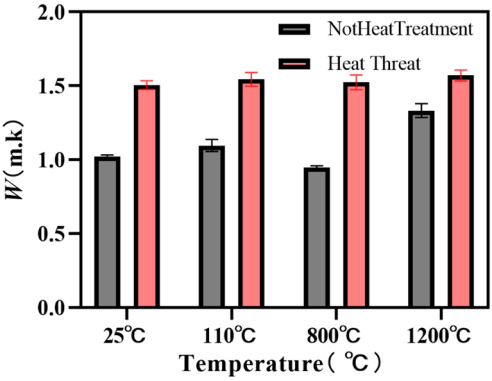

Fig. 5. Thermal Conductivity of Refractory Blocks After Use in the Combustion Chambe

The thermal conductivity of refractory materials [14] is closely related to the microstructure and chemical composition of the material (Figure.5). During the spraying and sintering process, the hydration products of aluminum phosphate and aluminate cement gradually dehydrate, transforming into pyrophosphate, metaphosphate, aluminum oxide, etc. , undergoing processes such as polymerization and polycondensation. Additionally, at high temperatures, the release of gases such as phosphorus oxide and water causes an increase in the micro-porosity of refractory materials. These factors result in a close correlation between the thermal conductivity of refractory materials and temperature.

The thermal conductivity of untreated refractory blocks ranges between 0. 949-1. 332 W/(m·K), with extreme values occurring at 800°C and 1200°C, respectively. After heat treatment, the thermal conductivity of refractory blocks stabilizes at 1.5 W/(m·K).

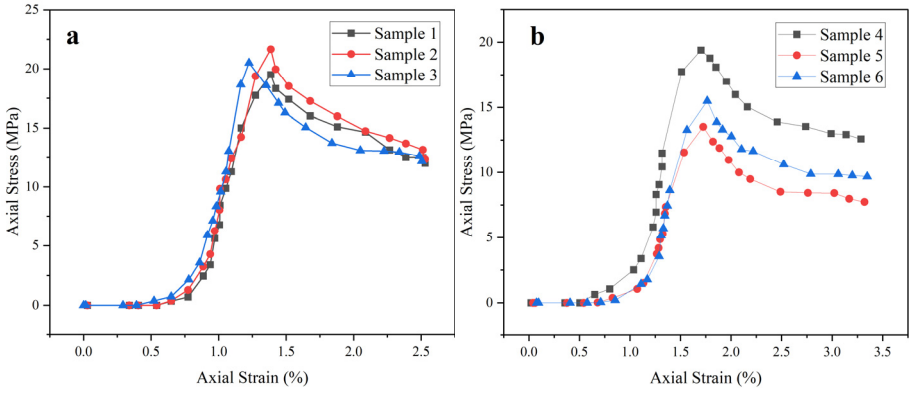

Fig. 6. Refractory Material Compressive Strength-Strain Curve (a) Untreated, (b) After Heat Treatment

Table 3. Peak Compressive Strength-Strain Indicators of Specimens

Not Heat Treatment		Heat Treatment	
Peak Axial Strain/%	Axial Stress/MPa	Peak Axial Strain/%	Axial Stress/MPa
1.26	19.5	1.70	19.4
1.38	21.67	1.72	13.5
1.22	20.5	1.76	15.5

The unconfined compressive stress-strain curve of refractory blocks is shown in Figure 6. Figure 6 indicates that the stress-strain curve of heat-treated refractory blocks follows a similar development trend to untreated refractory blocks and can be roughly divided into four stages:

Densification stage: The curve is concave upwards, representing the closure of internal pores under external force.

Elastic deformation stage: The curve is approximately a straight line.

Plastic development stage: In this stage, as strain continuously increases, the growth rate of stress gradually decreases until reaching the peak stress.

Failure stage: The curve shows a descending segment. The shape of the curve and the area it encloses with the coordinate axis reflect the ability of the specimen to dissipate energy. The descending segment indicates that the specimen still has a certain residual strength after reaching the peak load.

The Peak Compressive Strength-Strain Indicators of Specimens are show in Table 3. For untreated refractory blocks, the compressive strength values are 19.5, 21.67, and 20.5 MPa, with an average of 20.56 MPa. The compressive stiffness after heat treatment is 58. 49% of its original value. The peak compressive strength of heat-treated refractory blocks decreases by 21. 52%, and the strain corresponding to peak strength increases by 34. 2%.

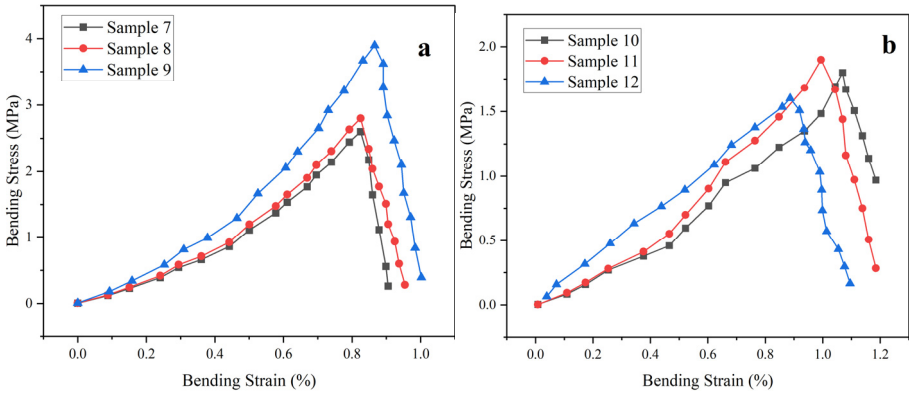

Fig. 7. Refractory Material Flexural Strength-Strain Curve (a) Untreated, (b) After Heat Treatment

Table 4. Peak Flexural Strength-Strain Indicators of Refractory Materials

Not Heat Treatment		Heat Treatment	
Peak Bending Strain/%	Bending Stress/MPa	Peak Bending Strain/%	Bending Stress/MPa
0.74	2.6	0.99	1.9
0. 82	2.8	0.88	1.6
0.86	3.9	1.12	1.8

The flexural stress-strain curve of refractory blocks is shown in Figure 6. When the component is subjected to bending, the lower part of the cross-section is in tension, while the upper part is in compression. After exposure to high temperatures, the internal porosity of refractory blocks increases. In the tensile region, under the action of tensile stress, cracks cut across the stress direction. The increase in cracks on the specimen reduces the effective area, leading to failure.

Figure 7 indicates that the flexural stress-strain curve of heat-treated refractory blocks follows a similar trend to untreated refractory blocks and can be divided into two stages:

Elastic stage: The flexural stress of refractory blocks increases with the increase of bending strain.

Failure stage: The flexural strength of refractory blocks decreases sharply after reaching the ultimate load due to the rupture of the specimen.

The Peak Flexural Strength-Strain Indicators of Refractory Materials are show in Table 4. For untreated refractory blocks, the flexural strength values from the start of loading to the peak point are 2.6, 2.8, and 3.9 MPa, with an average of 3.1 MPa. The peak flexural strength of heat-treated refractory blocks decreases by 43.01%, and the strain corresponding to peak strength increases by 24.2%.

4 CONCLUSIONS

This study investigated the influence of the high-temperature working environment of a natural gas ignition chamber on the performance of phosphate-bonded corundum refractory blocks. Conclusions drawn from experiments on the microstructure, composition, thermal conductivity, and mechanical strength of the refractory blocks include:

(1) Microstructure analysis revealed that the generated aluminum phosphate bonding phase was interspersed between the aggregate and matrix, providing the specimen with good mechanical properties. Under the high-temperature conditions of the combustion chamber, the decomposition of aluminate and aluminum phosphate occurred, forming Al_2O_3 and resulting in a porous structure with a loose framework.

(2) After high-temperature treatment in the combustion chamber, the internal structure and composition of the refractory blocks exhibit good thermal stability. Up to 1200°C, there is minimal change in volume and thermal conductivity.

(3) The change in strength characteristics of the refractory blocks is closely related to the hydration products of cement and the physical and chemical changes after heating. After the spraying treatment, the change in the compressive stress-strain curve of refractory blocks is roughly similar to the curve at room temperature. It can be divided

into stages of densification, elastic deformation, plastic development, and failure. Heat treatment resulted in a 21.52% reduction in the compressive strength of the refractory blocks.

(4) In contrast to compressive failure, the change in the flexural stress-strain curve of refractory blocks after spraying treatment is roughly similar to the curve at room temperature. It can be divided into elastic stage and failure stage. Heat treatment resulted in a 43. 01% reduction in the flexural strength of the refractory blocks.

Based on the field test of the combustion pool, this paper analyzes the change of material properties of the new aluminum phosphate bonded corundum refractory block under the condition of single heating. Due to the number and time of the combustion pool, the block test under complex working environment has not been carried out, and the influence of long-term multiple heating process on the block is still unknown. In the future, more field tests are planned to analyze the changes in masonry properties during complex multiple heating processes.

REFERENCES

1. Shaozhuan X. , Chuan H. , Jian C. , & Ping Y. (2023). Numerical Simulation of Natural Gas Combustion in Combustion Cell for Gas Production Test. *Journal of Southwest University of Science and Technology*, *38*(4), 73–79. https://doi. org/10. 20036/j. cnki. 1671-8755. 2023. 04. 010
2. Chen X. (2023). *Structural Design and Working Performance Study on New-type Prefabricated ombustion Masonry in Drilling Engineering* [D]. Southwest University of Science and Technology.
3. Ma K. (2021). *Development and Application of Natural Gas Sealed Combustion Unit* [D]. China University of Geosciences (Beijing).
4. Bayoumi, I. M. I. , Ewais, E. M. M. , & El-Amir, A. A. M. (2022). Rheology of refractory concrete: An article review. *Boletín de La Sociedad Española de Cerámica y Vidrio*, *61*(5), 453–469. https://doi. org/10. 1016/j. bsecv. 2021. 03. 003
5. Tomšů, F. , & Palčo, S. (2017). Refractory Monolithics versus Shaped Refractory Products. *Interceram - International Ceramic Review*, *66*(1), 20–23. https://doi. org/10. 1007/BF03401197
6. Xu, L. , Liu, Y. , Chen, M. , & Wang, N. (2022). An accurate correlation between high-temperature performance and cement content of the high-alumina refractory castables. *Ceramics International*, *48*(15), 22560–22566. https://doi. org/10. 1016/j. ceramint. 2022. 04. 273
7. Mamen, B. , Kolli, M. , Ouedraogo, E. , Hamidouche, M. , Djoudi, H. , & Fanttozi, G. (2019). Experimental characterisation and numerical simulation of the thermomechanical damage behaviour of kaolinitic refractory materials. *Journal of the Australian Ceramic Society*, *55*(2), 555–565. https://doi. org/10. 1007/s41779-018-0262-8
8. Kakroudi, M. G. , Yeugo-Fogaing, E. , Gault, C. , Huger, M. , & Chotard, T. (2008). Effect of thermal treatment on damage mechanical behaviour of refractory castables: Comparison between bauxite and andalusite aggregates. *Journal of the European Ceramic Society*, *28*(13), 2471–2478. https://doi. org/10. 1016/j. jeurceramsoc. 2008. 03. 048
9. Ouedraogo, E. , Roosefid, M. , Prompt, N. , & Deteuf, C. (2011). Refractory concretes uniaxial compression behaviour under high temperature testing conditions. *Journal of the*

European Ceramic Society, *31*(15), 2763–2774. https://doi. org/10. 1016/j. jeurceramsoc. 2011. 07. 017

10. Hachemi, S. , Khattab, M. , & Benzetta, H. (2023). Enhancing the performance of concrete after exposure to high temperature by coarse and fine waste fire brick: An experimental study. *Construction and Building Materials*, *368*, 130356. https://doi. org/10. 1016/j. conbuildmat. 2023. 130356
11. Lourenço, R. R. , Exposito, C. C. D. , Angélica, R. S. , & Rodrigues, J. A. (2010). Ação sonoquímica e influência das condições de tratamento térmico na preparação de cimentos do sistema binário CaO-Al2O3. *Cerâmica*, *56*, 28–38. https://doi. org/10. 1590/S0366-69132010000100006
12. Chen, D. , He, L. , & Shang, S. (2003). Study on aluminum phosphate binder and related Al2O3–SiC ceramic coating. *Materials Science and Engineering: A*, *348*(1), 29–35. https://doi. org/10. 1016/S0921-5093(02)00643-3
13. Scrivener, K. L. , Cabiron, J. -L. , & Letourneux, R. (1999). High-performance concretes from calcium aluminate cements. *Cement and Concrete Research*, *29*(8), 1215–1223. https://doi. org/10. 1016/S0008-8846(99)00103-9
14. Vitiello, D. , Nait-Ali, B. , Tessier-Doyen, N. , Rebouillat, L. , & Smith, D. S. (2022). Thermal conductivity of porous refractory material after aging in service with carbon pick-up. *Open Ceramics*, *11*, 100294. https://doi. org/10. 1016/j. oceram. 2022. 100294